Comparison of upstream Te profiles with downstream heat flux profiles and their implications on parallel heat transport in the SOL in DIII-D

M. A. Makowski, C. J. Lasnier, A. W. Leonard, G. Boedo, J. G. Watkins, D. N. Hill

May 21, 2010

Disclaimer

This document was prepared as an account of work sponsored by an agency of the United States government. Neither the United States government nor Lawrence Livermore National Security, LLC, nor any of their employees makes any warranty, expressed or implied, or assumes any legal liability or responsibility for the accuracy, completeness, or usefulness of any information, apparatus, product, or process disclosed, or represents that its use would not infringe privately owned rights. Reference herein to any specific commercial product, process, or service by trade name, trademark, manufacturer, or otherwise does not necessarily constitute or imply its endorsement, recommendation, or favoring by the United States government or Lawrence Livermore National Security, LLC. The views and opinions of authors expressed herein do not necessarily state or reflect those of the United States government or Lawrence Livermore National Security, LLC, and shall not be used for advertising or product endorsement purposes.

Comparison of upstream T_e profiles with downstream heat flux profiles and their implications on parallel heat transport in the SOL in DIII-D

M.A. Makowski[a][*], C.J. Lasnier[a], A.W. Leonard[b], J. Boedo[c], J.G. Watkins[d], and D.N. Hill[a]

[a]*Lawrence Livermore National Laboratory, Livermore, California 94550, USA*

[b]*General Atomics, P.O. Box 85608, San Diego, California 92186-5608, USA*

[c]*University of California-San Diego, La Jolla, California 92093, USA*

[d]*Sandia National Laboratories, Albuquerque, New Mexico 87185, USA*

Abstract

In DIII-D we measure the downstream target plate heat flux and relate it to Thomson and Langmuir probe profile measurements of n_e and T_e in the scrape-off layer (SOL) by projecting all measurements to the out-board midplane in order to assess the competition between parallel and cross-field heat transport. We analyze the measured characteristic widths associated with the SOL and model the results with the UEDGE code to provide insight into the mechanisms defining the various widths and the implications they have on transport.

Analysis of the scaling of the heat flux width reveals an essentially inverse dependence on I_p. The B_t dependence is extremely weak to non-existent. No dependence was found on the shear and normalized pressure gradient at the 95% flux surface (s_{95}, α_{95}), nor on P_{sol}, n_e or P_{inj}.

*Corresponding and presenting author address: General Atomics, P.O. Box 85608,

MS 13-153, San Diego, California 92186-5608, USA

*Corresponding and presenting author e-mail: makowski1@llnl.gov

I.   Introduction

Experiments were carried out in H-mode plasmas to measure the heat flux width, λ_q, as a function of various plasma parameters including magnetic field, B_t, plasma density, n_e, and injected power, P_{inj}. Care was taken to reduce the influence of ELMs through the use of ELM synchronization, a method of conditionally averaging results between ELM spikes over many ELM cycles. Heat flux and Thomson temperature and density profiles were all derived in this fashion.

Using this method, we have extracted gradient scale lengths of electron density and temperature at the midplane, and divertor heat flux widths. These, in turn, have been used to derive scaling laws and to examine parametric dependencies such as the relation of the heat flux width to the upstream electron temperature gradient scale length.

We have also started to model the experimental results with the UEDGE [1] code in an effort to understand the relative importance of cross-field and parallel transport.

II. Upstream Profiles

Upstream, ELM synchronized, edge profiles of n_e and T_e were measured with the Thomson scattering system, located at the upper outer region of the plasma at a major radius of 1.94 m. The profile typically consisted of 10-20 measurements within the 200 ms analysis window. The Thomson data was then mapped to the outer midplane. Simple exponential fits to the data immediately inside and outside the separatrix were made to obtain a measurement of the electron temperature gradient scale length, λ_{T_e}, which was then correlated with the heat flux width. Figure 1 shows typical profiles and exponential fits to both the core- and SOL-side data. It can be seen that the core-side exponential fit is influenced by the top of the pedestal. Scrape-off layer (SOL) widths from tanh-fits were also considered in the analysis. The trends reported below are independent of which parameter was used as the gradient scale length. To

be consistent with other published data, the SOL width has been used in the following.

III. Heat flux results

Heat flux to the lower divertor was measured with an IRTV camera mounted on the top of the vessel. Typically, a set of ~ 300 profiles were averaged to form a single heat flux profile. To facilitate comparison of the various profiles, they have all been mapped to the outer midplane.

These data were used to create a database by dividing each shot into segments 200 ms in length. Each of the plasma parameters was averaged over this interval. Additional parameters were also computed such as the shear and normalized pressure gradient at the 95% flux surface (s_{95}, α_{95}). Other parameters were included in the database to select good segments, since not all shot segments contained usable data.

Figure 2 shows a typical outer divertor heat flux profile as measured with the IRTV camera for $I_p = 0.52$ MA. The THEODORE code [2] was used to convert the temperature measured by the IRTV camera to a heat flux. For the profile shown, the THEODORE calculation was performed without carbon layers. Also shown are independent offset exponential $\left(a_0 + a_1 e^{x/\lambda}\right)$ fits to both sides of the heat flux profile. This procedure was necessitated since the low and high field sides of the heat flux profile had different baselines, likely resulting from radiative heating of the private flux region. This made the application of the standard definition of the Loarte width [3]

$$\lambda_q^{loarte} = \frac{\int q_{div}(r) 2\pi R dr}{2\pi R_{div} q_{div}^{peak}} \cdot \frac{R_{div} B_\theta^{div}}{R_{mp} B_\theta^{mp}}$$

difficult to apply. The heat flux width λ_q was taken as $\lambda_q = \lambda_{left} + \lambda_{right}$ which can be shown to be closely related to the Loarte width.

The measured heat flux width, λ_q, shows a very weak dependence on the upstream

3

T_e-profile regardless of which of the inferred gradient scale lengths was used. Figure 3 shows a plot of heat flux width versus the midplane T_e gradient scale length in the SOL. Due to the scatter in the upstream widths, the correlation coefficient is only 0.124 though, implying that the trend itself is weak. The observed trend is in strong disagreement with simple two-point models that predict $\lambda_{T_e} = (7/2)\lambda_q$ [4]. Given that the slope of the fit is almost zero, a slope of 7/2 predicted by the two-point model, appears to be nearly excluded by the data, despite the low correlation coefficient. The observed weak dependence of λ_{T_e} on λ_q is not an unreasonable result since radial transport, SOL radiation, and divertor recycling affect heat flux within flux tubes; effects not taken account of in the models leading to the cited scaling law.

A variety of multi-parameter fits were attempted to establish scaling laws between the heat flux width, λ_q, and I_p, q_{95}, n_e, B_t, P_{sol}, P_{inj}, s_{95}, and α_{95}. The only significant dependence found was on I_p. The dependence of λ_q is nearly inverse, scaling as $I_p^{-1.24}$ as shown in Fig. 4. The B_t scaling previously reported [5] was not observed in this data. This may be due to the fact that the influence of ELMs was eliminated in this data set through the use of inter-ELM averaging. Also, there were only a limited number of low-field data points in the current data set.

IV. Other scaling laws

There are a number of multi-machine scaling laws in existence. Here we consider two. The first is the JET conduction limited scaling law [6] given by

$$\lambda_q^{JET}(\text{mm}) = 2.41 \times 10^{-5} B_T^{-1}(\text{T}) P_{SOL}^{-1/2}(\text{MW}) n_e^{1/4} \left(\text{m}^{-3}\right) q_{95} R^2 (\text{m}).$$

This is in quite good agreement with data from the DIII-D experiment. Figure 5 shows a plot of λ_q^{DIII-D} versus λ_q^{JET}. The bulk of the dependence results from the variation in

4

$q_{95}/B_t \sim 1/I_p$. The factor $n_e^{1/4}$ has little influence on the scaling law and no dependence on n_e has been found in our data. The $n_e^{1/4}$ scaling on density is quite weak at any rate. Further, we also observe no dependence on P_{sol}, though the scaling law has a $P_{sol}^{-1/2}$ dependence. Since R is a constant for our data, the scaling law reduces to $\lambda_q^{JET} \sim B_t^{-1} q_{95} \sim 1/I_p$, which essentially the scaling shown in Fig. 4.

We have also considered the multi-machine scaling law from reference [2]:

$$\lambda_q^{H-2}(mm) = 5.3 P^{0.38}(MW) B_T^{-0.71}(T) q_{95}^{0.30}.$$

☐This is in extremely poor agreement with the DIII-D data and predicts profile widths a factor of 10 lower than those measured in DIII-D. There is no size dependence and the dependence on q_{95} is rather weak.

V.   UEDGE simulations

Efforts are underway to model four representative points on the I_p scan of Fig. 4 with UEDGE [1] in order to determine what underlying physics might be changing with I_p to affect λ_q. Inputs to UEDGE are the power flux through the SOL and the midplane electron temperature and density profiles. Transport coefficients are adjusted within UEDGE to obtain a match between the upstream experimental Thomson profiles and UEDGE profiles and held fixed thereafter. Results are preliminary but still offer some insight. The results reported below are with the flows partially turned on (20% of their full value). Figure 6 shows a comparison of the measured heat flux profile and that obtained from a UDEGE simulation as a function of distance along the target plate for $I_p = 1.5$ MA. The measured profile is scaled by a factor of 5.2 and is thus much lower than that predicted by UEDGE.

With the drifts turned off only ~ 90 kW of power is radiated in the divertor, which is much less than the experimentally measured value of 350 kW. This is caused by a very high value

of electron temperature and low value of electron density at the target plate. The high temperature also leads to a large radial electric field that in turn leads to a strong $\mathbf{E} \times \mathbf{B}$ poloidal flow. The flow, in turn, increases n_e at the plate with a corresponding increase in radiated power. With the flows partially turned on better agreement in the power balance is obtained with ~ 300 kW of radiated power predicted by UEDGE in this case. The UEDGE heat flux profile width is about 25% narrower than the measurement without the flows turned on. With the flows partially turned on, the heat flux width broadens, but is still narrower than the experimental profile. Note that a shoulder is developing on the rhs corresponding to the shoulder in the experimental data. No in/out asymmetry of the baseline is present on the UEDGE profile in contrast to the measurement.

VI. Summary

We have measured upstream electron temperature and density profiles and derived gradient scale lengths from them. These have been related to the measured downstream heat flux widths and a very weak dependence between them has been found between the two quantities. The dependence is much weaker than simple two-point models would predict. A scaling law for the DIII-D heat flux width has been developed and is only dependent on $I_p^{-1.24}$. This is in very good agreement with JET scaling law that takes size into account. UEDGE runs are currently in progress and beginning to yield some insight into the mechanisms influencing the heat flux width. It is already clear that the plasma flows play a significant role in the shaping of the heat flux profile.

References

[1] T. Rognlien, *et al.,* J. Nucl. Mater. **196-198** (1992) 347-351.

[2] A. Hermann, *et al.*, Plasma Phys. Control. Fusion **37** (1995) 17.

[3] A. Loarte, *et al.,* J. Nucl. Mater. **266-269** (1999) 587-592.

[4] C.S. Pitcher and P.C. Stangeby, Plasma Phys. Control. Fusion **39** (1997) 779.

[5] C. Lasnier, *et al.,* in Proc. 36th EPS Conf. on Plasma Physics, Sofia, Bulgaria, June 29 - July 3, 2009 ECA Vol.33E, P-4.140 (2009).

[6] G. Kirnev, *et al.*, Plasma Phys. Control. Fusion **49** (2007) 689.

Figure Caption

Fig. 1. Upstream T_e and n_e profiles mapped to the outer midplane. Fits to exponentials on both the core and SOL sides of the profile are shown. The SOL side fit was used as a measure of the upstream profile gradient scale length.

Fig. 2. Typical heat flux profile as a function of major radius relative to the location of the separatrix at the midplane, $R - R_{sep,mp}$. Also shown in red are offset exponential fits to both sides of the profile.

Fig. 3. Plot of the heat flux width, λ_q, versus the Thomson profile e-folding length in the scrape off layer, $\lambda_{Te,sol}$. Solid red line is a linear fit between the two parameters. The slope, s, is 1/10th that predicted by simple two-point models.

Fig. 4. Plot of the heat flux width, λ_q, versus I_p for two ranges of B_t (red and blue curve fits). Due to the weak dependence of λ_q on B_t, the two curves nearly overlap. The black line is fit to all the data (red and blue circles).

Fig. 5. Plot of λ_q^{DIII-D} versus λ_q^{JET} showing that the DIII-D fits the JET scaling law.

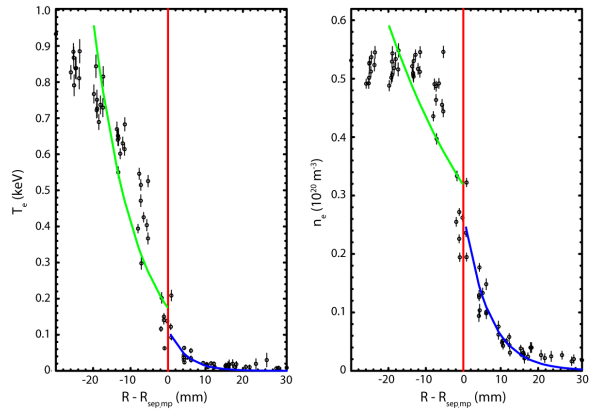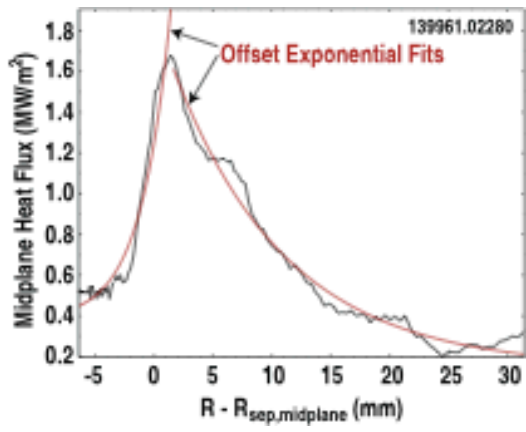Fig. 6. Comparison of measured heat flux (blue, multiplied by 5.2) and that predicted by UEDGE (blue). For this case $I_p = 1.5$ MA.
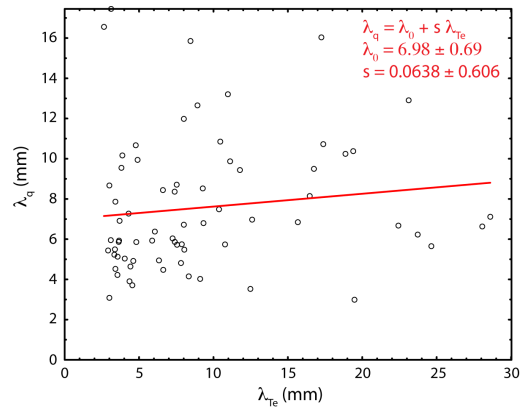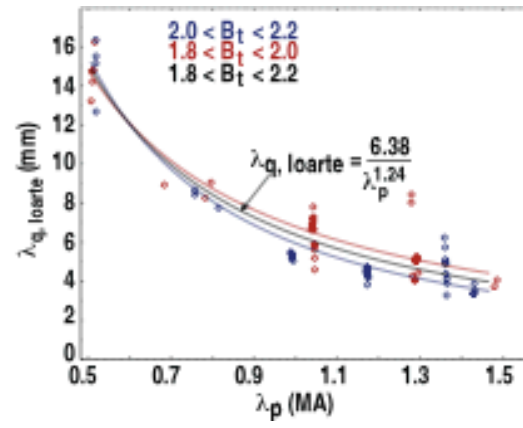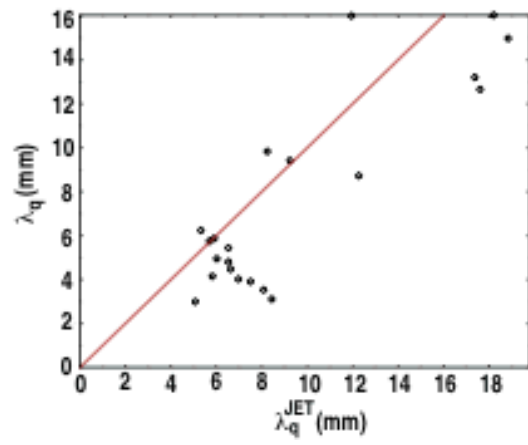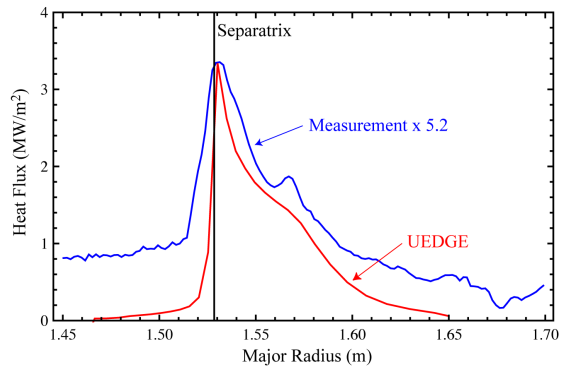
Figure 1

Figure 2

Figure 3

Figure 4

Figure 5

Figure 6